ACCSCIENCE PUBLISHING

Artificial Intelligence in Health

ORIGINAL RESEARCH ARTICLE

Screening and early detection of cervical intraepithelial neoplasia and cervicitis using a hemoglobin absorption map-derived machine learning algorithm

Phebe George[1], Rekha Upadhya[2], Rinoy Suvarnadas[1], Niranjana Sampthalia[3], and Subhash Narayanan[1]*

[1]Research and Development Division, Sascan Meditech Pvt. Ltd., TIMed, Sree Chitra Tirunal Institute for Medical Sciences and Technology, Thiruvananthapuram, Kerala, India

[2]Department of Obstetrics and Gynaecology, Kasturba Medical College, Manipal Academy of Higher Education, Manipal, Karnataka, India

[3]Department of Biomedical Engineering, Manipal Institute of Technology, Manipal Academy of Higher Education, Manipal, Karnataka, India

Abstract

Early and non-invasive detection of cervical malignancy holds great clinical significance. Diffuse reflectance (DR) spectroscopy has the capability to map tissue transformation at the biochemical, morphological, and cellular levels. We have developed a non-invasive, multimodal imaging system to map changes in tissue autofluorescence using DR for the screening and early detection of cervical cancer and cervical inflammation (cervicitis). The developed multispectral imaging device consists of light-emitting diodes (LED) emitting at 375, 545, 575, and 610 nm wavelengths, along with a 5-megapixel monochrome camera for image acquisition. Camera operation and image analysis are controlled using proprietary software installed on a Windows tablet. The 375 nm LED-excited autofluorescence, and the elastically backscattered light at 545, 575, and 610 nm originating from the cervix tissue are captured by the camera and processed to assess tissue abnormalities. A machine learning (ML) algorithm based on DR image intensity ratio values was developed for tissue classification. It was observed that the R610/R545 image ratio could discriminate malignant cervical sites from normal tissues, achieving a sensitivity of 100% and specificity of 93%. In comparison, cervicitis could be discriminated from normal tissues using the R610/R575 ratio, with a sensitivity of 91.6% and specificity of 94.4%. The study demonstrates the potential of DR imaging in conjunction with ML algorithm to non-invasively screen and detect cervical intraepithelial neoplasia and cervicitis in real time. As compared to the existing practice of Pap smear and colposcopy-directed biopsy, which are subjective and require a waiting period for results, objective screening using CerviScan would help reduce patient anxiety, unnecessary biopsies, and treatment costs. With increased patient screening, the accuracy of the ML algorithm would improve. When integrated into a cloud server, the system could address the needs of multiple users in a field setting.

Keywords: Cervical intraepithelial neoplasia; Cervical inflammation; Diffuse reflectance image intensity ratio; Machine learning algorithm

***Corresponding author:**
Subhash Narayanan
(subhash@sascan.in)

Citation: George P, Upadhya R, Suvarnadas R, Sampthalia N, Narayanan S. Screening and early detection of cervical intraepithelial neoplasia and cervicitis using a hemoglobin absorption map-derived machine learning algorithm. *Artif Intell Health*. 2025;2(3):125-137. doi: 10.36922/aih.8527

Received: January 14, 2025

Revised: March 6, 2025

Accepted: April 10, 2025

Published online: May 2, 2025

1. Introduction

Cervical cancer is the most common type of cancer affecting women and one of the major public health problems in the world.[1] While it is manageable if detected early, cervical cancer continues to be a leading cause of cancer-related death – particularly in underdeveloped countries – where higher mortality rates are often observed among women from low socioeconomic backgrounds.[2] According to the World Cancer Report 2020, India reports one-fifth of the global burden of cervical cancer,[3] and the disease is the major cause of mortality in countries with a low Human Development Index.

Despite the high mortality rates, cervical cancer is one of the most preventable types of cancer due to its slow progression, the presence of detectable lesions using cytology, and the availability of effective treatments.[4] However, cytology-based Pap smear tests inherently have low sensitivity (<50%) and specificity (60 – 70%).[5] Furthermore, the accuracy of the diagnosis depends on the expertise and skill of the gynecologist collecting the exfoliated cervical cells. The presence of blood, the absence of squamous-columnar junction cells, or the clustering of the cells may interfere with the cytology results. These factors contribute to a high number of false negatives or undetected cases of early-stage or low-grade squamous intraepithelial neoplasia (LSIL) that have a favorable prognosis.

Positive Pap cases are typically referred for conventional visual inspection with acetic acid method of examination, and colposcopy-guided biopsies are considered the gold standard for cervical cancer detection. However, these tests are inherently subjective in nature, with the selection of the most malignant or abnormal site depending on the clinician's expertise.[6] Furthermore, there is a long waiting period before pathology results become available for patient care. Thus, there is a long-felt need for screening tests that are objective, with improved diagnostic accuracy for the detection of LSILs in real time. Factors including lack of awareness, discomfort during the screening procedure, and the need for multiple visits prevent women from periodic screening.[7] A non-invasive and low-cost modality that provides real-time screening results is essential to make women come forward for periodic check-ups. This would enable early detection of the disease, leading to a reduction in the mortality rates over time. With the introduction of vaccines against human papillomavirus (HPV) infection, cervical cancer prevention has undergone dramatic changes over the past decade. Although some countries have seen a decline in HPV-mediated cervical disease, widespread implementation of vaccination is limited by economic considerations, vaccine availability, and vaccine adoption hesitancy among the population.

Cervicitis refers to inflammation of the cervical tissue. This could be asymptomatic or symptomatic, including vaginal discharge, bleeding, and irritation, as well as intermenstrual or postcoital bleeding and lower abdominal pain. Cervicitis can be caused by either bacteria such as *Chlamydia*, *Gonorrhea*, and *Trichomoniasis*, or non-infectious exposure to chemicals, including condoms, tampons, and cervical caps. The current diagnosis of cervicitis is the same as for cervical cancer.

When light falls on tissue, various processes such as absorption, reflection, refraction, transmission, and scattering occur. The absorption and scattering properties of light depend on the tissue's internal structure, layer thickness, biochemical constitution, and the wavelength of the incident light. Therefore, spectroscopy-based techniques – such as those utilizing tissue fluorescence, scattering, and diffuse reflectance (DR) – are effective in identifying the structural, morphological, and biochemical changes in cervical tissues during cancer development.

The hemoglobin (Hb) and oxyhemoglobin (HbO_2) have distinct absorption spectral features in the visible spectrum, with HbO_2 showing two distinct peaks around 545 nm and 575 nm. However, Hb exhibits a higher molar extinction coefficient in the 600 – 650 nm spectral range compared to HbO_2.[8] This differential absorption cross-section can be utilized to discriminate between normal and abnormal cervical tissues.

Studies have been conducted to assess the potential of DR spectroscopy in discriminating cervical cancer. The chromophore Hb has absorption peaks around 280 nm, 420 nm, 540 nm, and 580 nm.[9] The DR spectrum of cervical tissues exhibits changes in the HbO_2 absorption at 542 nm and 577 nm due to a reduction in heme production during malignant transformation.[10,11] Shaikh *et al.*[12] cross-validated the DR technique with Raman spectroscopy to compare the classification accuracy for the detection of tumor sites in normal patients. In another clinical study, Prabitha *et al.*[13] reported an increase in the R545/R575 image intensity ratio with an increase in the grade of cervical cancer. Similarly, the DR image ratio R545/R575 was used in the detection of early-stage malignancies in the oral cavity with good diagnostic accuracy.[14,15]

Prasanth *et al.*[16,17] also utilized DR spectral measurements and multispectral imaging techniques to detect gingivitis and periodontitis in patients with gum inflammation. Significant changes in the recorded spectra were observed at 545 nm and 575 nm with gingival inflammation, and the DR spectral ratio R620/R575 was found to give a good correlation with different grades of gingival inflammation. A sensitivity of 91.6% and a specificity of 93% were observed in discriminating healthy and mildly inflamed

gingiva using the R620/R575 image intensity ratio. In another study, the R620/R575 spectral ratio was able to discriminate between healthy gingiva from gingivitis, with 90% sensitivity and 94% specificity, whereas a sensitivity of 91% and a specificity of 100% were obtained when discriminating gingivitis from periodontitis.[18] Recently, Barik *et al.*[19] recorded the fluorescence emission of the cervix on excitation at 325 nm, and the spectral features were used to discriminate dysplasia from inflammatory changes. An increase in fluorescence emission intensity in cervicitis samples was observed at 435 nm compared to normal tissue, which was attributed to the fluorophore nicotinamide adenine dinucleotide. Zhang *et al.*[20] utilized a feature fusion method to extract information from Raman spectra and its derivatives. They classified inflamed cervical tissues as high-grade squamous intraepithelial lesions and LSIL based on the intensity of the prominent spectral peaks at 548, 640, 1,452, and 1,664 cm^{-1}. In another study, colposcopy images, in conjunction with deep learning, achieved an accuracy of 95.2% in discriminating chronic cervicitis from cervical cancer.[21]

A recent study combining fluorescence and DR imaging for the detection of oral cavity lesions reported improved diagnostic accuracy in discriminating potentially malignant oral lesions from normal tissues. This was achieved using a machine learning (ML) algorithm based on the DR image ratio R620/R545, which represents changes in the deoxy to oxygenated Hb absorption in tissue.[8] The study highlights the effectiveness of non-invasive screening modalities to provide real-time user feedback and to enhance compliance, particularly for the early detection of cervical cancers.

In the past decade, ML models have been widely used for medical diagnosis. Dong *et al.*[22] developed an ML model for cervical cancer risk stratification using full-genotyping of high-risk HPV test data. The study compared four ML models zs– XGBoost, support vector machine (SVM), random forest, and naïve Bayes – where the XGBoost model was found to be the most effective model.

Surface plasmon resonance biosensor with ML optimization was developed by Wekalao *et al.*[23] for cervical cancer detection. This support vector regression was found to enhance the sensor's predictive capability, reducing the stimulation time by 80%. Several deep learning techniques have been used for cervical cancer diagnosis using pathology slides and colposcopy images.[24]

As part of this study, we have developed a multispectral imaging system for multimodal imaging of the cervix. With the help of an ML algorithm, the DR imaging system evaluates the accuracy of the DR image ratios, R610/R545 and R610/R575, for the detection of cervical cancer and cervicitis, respectively. The study conducted using this device demonstrates its potential for real-time tissue status assessment and its ability to detect the most malignant site for biopsy. The DR image ratios were correlated with the histopathology results of guided biopsies to develop an ML algorithm. The diagnostic accuracy of the screening was determined from the scatter plot diagrams, and the results were presented accordingly.

2. Materials and methods

2.1. Methodology

The CerviScan (Figure 1) consisted of a bimodal imaging camera designed for fluorescence and DR imaging of the cervix. The device was equipped with a 5-megapixel monochrome camera (MU9PM-MH, Ximea, GmbH, Germany) to record the fluorescence emission of collagen on excitation with 370 nm LEDs (ATS2012UV365, Kingbright, United States). The HbO_2 absorption changes in cervical tissues were assessed from the DR images captured under illumination with LEDs emitting at 545 nm (L1C1-GRN1000000, LUMI LEDs, Netherlands) and 575 nm (SMP2-SGC, Bivar, United States), with both overlapping the HbO_2 absorption spectra at 542 nm and 577 nm. The DR images were also captured following LED illumination at 610 nm (SMP2-SOC, Bivar, United States), where the absorption changes in cervical tissues due to Hb were stronger compared to HbO_2. A Windows tablet (Chuwi, China) was connected to a USB camera (Ximea, GmbH, Germany), with proprietary software installed for camera control, image capture, and analytics. The monochrome images (Im545, Im610, Im575, and F370) recorded were processed by software in real time to generate ratio images (R610/R545 and R610/R575) and their corresponding pseudocolor maps (PCM). The region of interest (ROI) was then marked on these ratio

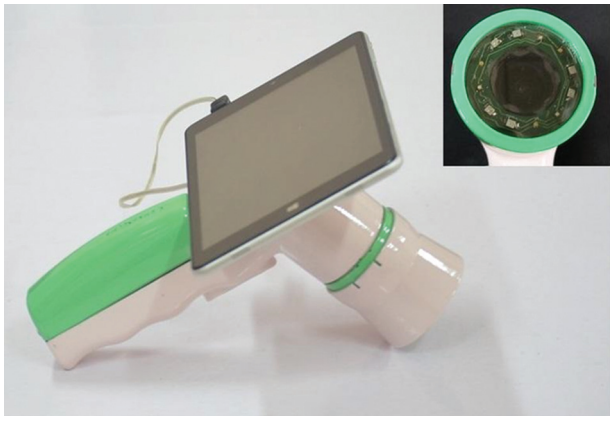

Figure 1. Hand-held CerviScan device developed for cervical cancer detection. The inset shows the front view of the device with the light-emitting diodes positioned around the camera.

images, with reference to the pseudocolor intensity maps of autofluorescence and the DR images displayed on the screen. The software detected and marked the site with the highest ratio value in the abnormal area or ROI. A biopsy was obtained from this site, and the results were correlated with the histopathology findings.

Before the initiation of the imaging procedure, the camera sensor was calibrated to the ambient light conditions using a tissue phantom. The device was positioned at a working distance of 15 cm from the tissue phantom, and the calibration icon in the software was clicked. The four sets of LEDs blinked sequentially until the calibration was successfully completed. During the calibration process, the shutter speed of the imaging camera was adjusted relative to the LED intensity to accommodate the dark room conditions to provide the same levels of image contrast, as verified in the captured image following the calibration procedure. A calibration window appeared after the calibration was successfully completed. The device needs to be recalibrated when there is a change in the room light intensity.

2.2. Study design and patient enrollment

The clinical study was conducted at the Department of Obstetrics and Gynecology, Kasturba Medical College, Manipal, India, after obtaining approval from the Institutional Ethics Committee (Ref no. 152/2020). This trial was also registered with the Clinical Trial Registry of India (REF/2020/08/036212).

Study participants were enrolled according to the study's inclusion criteria. Women who were referred for a Pap smear test and those with clinically suspicious lesions in their cervix were included in the study. Women with transmittable diseases and those who had previously received treatment for cervical cancer were excluded from the study. Signed informed consent was obtained from all participants before the initiation of any examination procedures.

2.3. Data acquisition

The patient was asked to lie down in the supine lithotomy position. After cleaning the vaginal area with a soft cotton swab, the gynecologist inserted a speculum for proper visualization of the cervix. A colored photo of the cervix was taken as a reference. The CerviScan device was held steadily and moved back and forth to obtain a focused image on the screen. The capture switch on the device was pressed, and four monochrome images of the cervix were recorded and stored in the computer following sequential illumination at 370 nm, 545 nm, 575 nm, and 610 nm wavelengths. The captured images were reviewed for clarity, and if required, the images were recaptured. The imaging of the entire cervix enabled clinicians to identify the optimal areas for further investigation.

The cervical smear was collected from the patients referred for Pap smear testing using a cervical broom and sent for cytology examination. Women with clinically suspected cervical malignancy underwent either a conventional or colposcopy-guided cervical biopsy. The site for the biopsy was decided based on the visual impression and the gynecologist's experience. The cervix was anatomically labeled using clock positions, with the anterior tip at the 12 o'clock position and the posterior tip at the 6 o'clock position. The cervical arteries and veins run parallel in 3 and 9 o'clock positions, and biopsies were generally avoided in this area.

2.4. Data processing

Figure 2 illustrates the data processing workflow of CerviScan. In the first step, the camera captured four monochrome images. In the pre-processing step, the software created pixel-by-pixel ratio images of DR-recorded images (R610/R545 and R610/R575). The PCMs of these ratio images, along with the PCM of the F375 (fluorescence) image, were displayed from blue to red, with increasing grades of malignancy. For feature extraction, the areas of the cervix with clinical significance were identified by adjusting the color bar in the PCM image of tissue autofluorescence and the DR ratio image (R610/R545), followed by marking the ROI on either the fluorescence or DR ratio images. In the post-processing, the software identified the highest ratio value in the marked ROI for abnormal tissues and an average of the values for normal tissue. The program identified the most malignant site within the ROI by locating the pixel with the highest ratio value.

3. Results

A total of 109 patients were recruited for this study. Out of the study population, 42 patients with histopathology results were included in the analysis (Table A1). The results of histopathology and cytology were correlated with the R610/R545 ratio values of the biopsy site. The patients who underwent hysterectomy following a negative Pap smear test were also included as healthy subjects. The results of histopathology or cytology were correlated with the R610/R545 ratio values of the biopsy sites. The processed DR image ratio R610/R575 was analyzed to discriminate cervicitis from normal tissues.

3.1. Case studies

The severity of the disease in the cervix was assessed based on the percentage increase in the DR ratio R610/R545 value compared to that of the normal cervix. Low DR

ratio values indicate normal tissues, while higher ratio values represent higher grades of malignancy. The most malignant site was identified as a site with the highest DR image ratio R610/R545 value, and a biopsy was obtained from this site for an accurate determination of the cancer grade through histopathology.

Typical cases of patients with cervical intraepithelial neoplasia (CIN) and one case of cervicitis are presented below:

3.1.1. Case 1

Figure 3 shows a 56-year-old patient with complaints of post-menopausal bleeding and abdominal pain. The gynecologist identified a massive growth covering the anterior and posterior lips of the cervix and the upper part of the vagina. The patient was diagnosed with squamous cell carcinoma based on a Pap smear test. A conventional biopsy was obtained from the growth. Our device recorded a R610/R545 ratio value of 2.078. The histopathology result diagnosed the disease as grade 2 squamous cell carcinoma.

3.1.2. Case 2

This is the case of a 50-year-old patient presenting with foul-smelling discharge and blood stains for the past 2 years, along with passage of clots, abdominal pain, general weakness, and loss of appetite. The physical examination showed an irregular mass on the anterior side of the cervix, with the involvement of the posterior and lateral fornix, as well as the lower part of the vagina. The histopathology result following cervical biopsy confirmed malignancy. Immunohistochemistry and immunofluorescence, along with histopathology results, confirmed the diagnosis of carcinosarcoma (squamous cell carcinoma with sarcoma), with an R610/R545 image ratio value of 3.005, as illustrated in Figure 4.

3.1.3. Case 3

A 50-year-old patient with cervicitis was studied based on the DR image ratio R610/R575 value. The patient had difficulty in passing urine, and her cervix showed erosions (Figure 5). Based on the biopsy results, the patient was diagnosed with chronic cervicitis and no dysplasia. This case demonstrated a relatively higher R610/R575 ratio value of 2.433, compared to a lower R610/R545 ratio value of 1.461.

3.2. Scatter plot and algorithm development

The scatter plot diagram of the R610/R545 ratio values, correlated with the corresponding pathological results, was used to classify normal and malignant cervical tissues

Figure 2. Block diagram of data processing and analysis using CerviScan

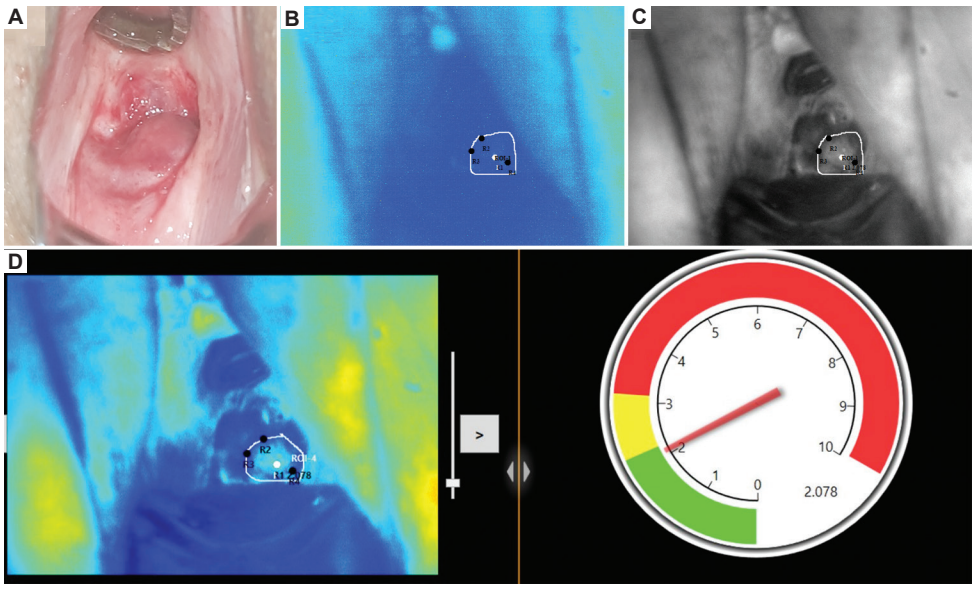

Figure 3. Images of grade 2 cervical carcinoma: (A) Clinical impression, (B) pseudocolor fluorescence, (C) monochrome diffuse reflectance image ratio R610/R545, and (D) pseudocolor diffuse reflectance image ratio R610/R545, with a dial indicating a ratio value of 2.078 in the marked region of interest

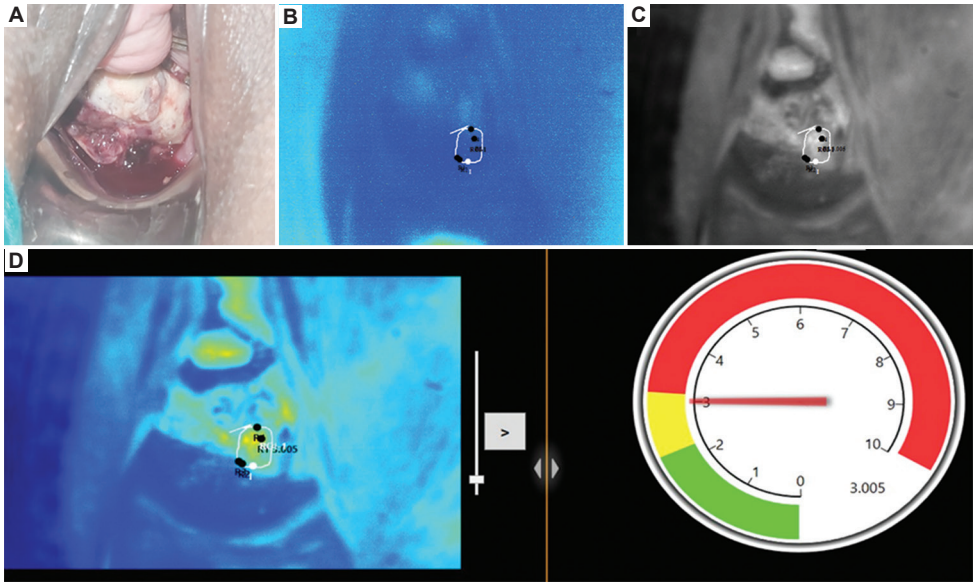

Figure 4. Images of cervical carcinosarcoma: (A) Clinical impression, (B) pseudocolor fluorescence, (C) monochrome diffuse reflectance image ratio R610/R545, and (D) pseudocolor diffuse reflectance image ratio R610/R545, with a dial indicating a ratio value of 3.005 in the marked region of interest

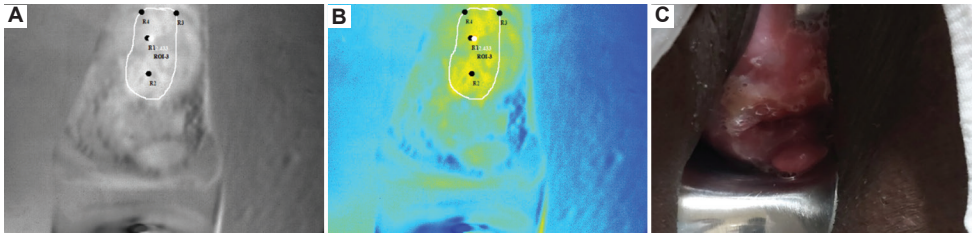

Figure 5. Patient with chronic cervicitis: (A) Monochrome diffuse reflectance image ratio R610/R575 with marked region of interest, (B) pseudocolor diffuse reflectance image ratio R610/R575, and (C) clinical image of the cervix

(Figure 6). The discrimination line was drawn at 1.470, which is the average DR ratio value of all normal and abnormal sites. Patients with no dysplasia were classified as normal. Among 27 normal cases, three cases were misclassified as abnormal, whereas all malignant cases were correctly classified, leading to a specificity of 88% and sensitivity of 100%. The mean DR ratio value for normal sites was 1.367, whereas the mean DR ratio value for all malignant cases was 1.871.

Figure 7 shows the scatter plot of the R610/R575 image ratio used to discriminate cervicitis from the normal cervix. There were 18 patients in the normal group, with an average R610/R575 ratio value of 1.266, whereas the abnormal group of 17 patients with cervicitis showed an average R610/R575 ratio value of 1.663. Tissue classification was carried out by drawing the discrimination line at 1.459, representing the mean R610/R575 ratio for all normal (1.266) and abnormal cases with cervicitis (1.663). None of the malignant cases were included in this classification. Using the R610/R575 ratio, a sensitivity of 70.58% and

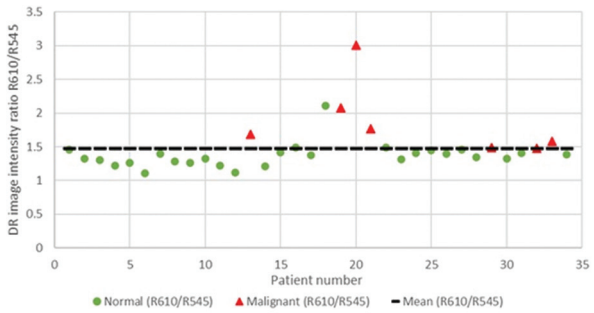

Figure 6. Scatter plot algorithm of DR image intensity ratio R610/R545 used to classify normal and malignant tissues, with a discrimination line drawn at the mean ratio value of 1.47
Abbreviation: DR: Diffuse reflectance.

specificity of 83.33% were achieved in discriminating cervicitis from normal tissues.

The key features of the ML algorithm were in regard to its potential for mapping changes in HbO_2 absorption, quantifying tissue abnormalities, and biopsy guidance. The

key inputs to this algorithm were the ratio values derived from the images of the cervix. The processed ratio images (R610/R545 and R610/R575) were used as the primary feature for classification. The R610/R545 ratio value-based algorithm classifies cervical tissues as normal or malignant, while the R610/R575 ratio value-based algorithm classifies cervical tissues as normal or cervicitis. The model was trained using histopathology-verified datasets from 109 patients, with 35 biopsy-confirmed cases. The model provides feedback to the clinician or its user in real-time and provides biopsy guidance. It was observed that the increase in the R610/R545 ratio value correlated with the malignant status of the tissues, whereas the increase in the ratio R610/R575 correlated with cervicitis. The collagen fluorescence intensity was expected to decrease in malignant sites, and the decreasing trend was presented on screen as a PCM.

The receiver operator characteristics (ROC) curves were plotted for the R610/R545 ratio value algorithm to discriminate normal tissues from malignant tissues, and the R610/R575 ratio to discriminate normal tissues from cervicitis (Figure 8). The area under the curve was found to be 0.957 for the ROC of R610/R545 ratio and 0.803 for the ROC of R610/R575 ratio, classifying normal tissues from malignant tissues and normal tissues from cervicitis, respectively.

The box plot (Figure 9) represents the distribution of R610/R545 image intensity ratio values for normal and malignant tissues. The horizontal line inside the box represents the median of both data sets. The wider box for malignant samples suggests a larger variation in intensity values compared to normal samples. The malignant samples demonstrated higher intensity values compared to the normal samples. This suggests a significant difference in the R610/R545 image intensity ratio between normal and malignant cervix arising from the pathological changes.

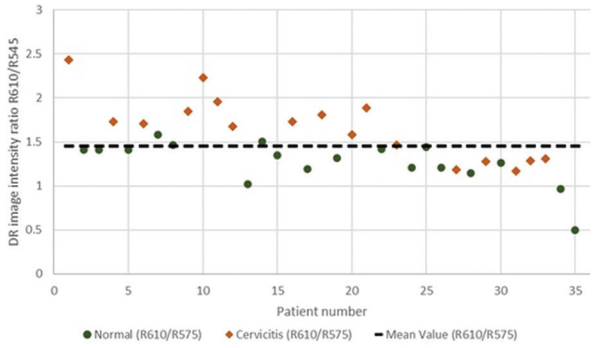

Figure 7. Scatter plot algorithm of DR image intensity ratio R610/R575 used to classify normal tissues and cervicitis, with a discriminating line drawn at the mean ratio value of 1.459
Abbreviation: DR: Diffuse reflectance.

4. Discussion

In this study, a combination of DR and fluorescence imaging was used to identify cervical abnormalities. The higher percentage variance in R610/R545 ratio values highlights the device's ability to detect cervical precancers in a clinical setting. In histopathology, patients with cervicitis but no dysplasia were classified as unhealthy for cervicitis classification; however, these patients were considered normal for the R610/R545 image ratio classification.

In a clinical study conducted by Prabitha *et al.*,[10] it was reported that absorption at 542 nm and 574 nm in the DR spectrum due to HbO_2 becomes stronger owing to reduced heme production in malignant tissues, whereas no significant change in intensity was observed at 610 nm. Stephen *et al.*[15] pointed out that the heme production in malignant tissues is altered as a result of the reduced

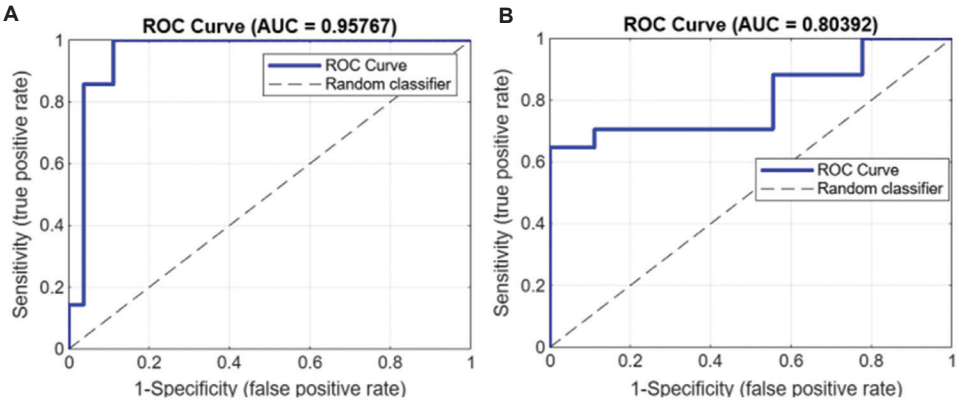

Figure 8. ROC-AUC for image intensity ratios: (A) R610/R545 ratio for normal tissues versus malignant tissues, and (B) R610/R575 ratio for normal tissues versus cervicitis
Abbreviations: AUC: Area under curve; ROC: Receiver operator characteristics.

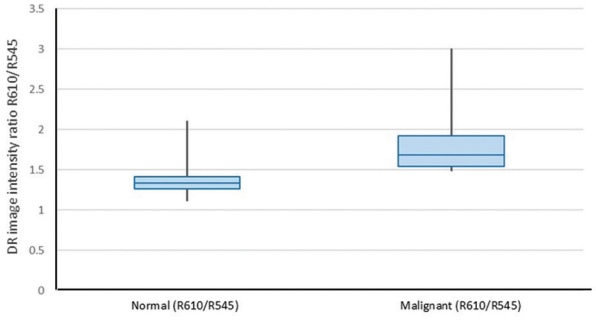

Figure 9. Box plot representing the distribution of DR image intensity ratio (R610/R545) value for normal and malignant tissues
Abbreviation: DR: Diffuse reflectance.

activity of the ferrochelatase enzyme. This leads to lower Hb production and, consequently, lower absorption at the HbO_2 absorption peak. Our study showed a linear relationship between the R610/R545 image ratio value with tissue status (Table A1), highlighting the potential of the R610/R545 image ratio to discriminate between healthy and cancerous lesions of the cervix. In line with our results, Narayanan *et al.*[8] reported a sensitivity of 82.2% and specificity of 96.63% for the R610/R545 image ratio to discriminate oral potentially malignant lesions from normal tissues.

In this analysis, squamous metaplasia occurring at the squamocolumnar junction was considered healthy. Two patients (No. 19 and 21 in Table A1) diagnosed with squamous metaplasia were classified as true negatives, with an average DR image ratio (R610/R545) value of 1.397. Endometrial adenocarcinoma was reported in one patient (No. 22 in Table A1); however, the biopsy results confirmed that the cervix was free from carcinoma. The R610/R545 image ratio value of this patient was 2.11 and was classified as false positive. Case 2 represents carcinosarcoma, a malignancy involving the epithelial and mesenchymal parts of the cervix.[25] Although this disease is reportedly challenging to diagnose, the device recorded the highest DR image ratio value of 3.005, suggesting its ability to discriminate between normal and carcinosarcoma tissues.[26]

As this was a pilot trial, only a small number of patients were recruited for this study. However, with more patients enrolled, the scatter plots developed for determining the sensitivity and specificity of detection could progress to a cloud-based ML algorithm that could classify tissue inflammation and different grades of cancer/CIN from normal tissues. Point-of-care detection of cervical diseases, made possible through a cloud-based ML algorithm, would establish CerviScan as a low-cost alternative for population-based screening. With a greater number of users sharing their screening data and pathology results with the ML algorithm, its robustness in providing feedback on tissue status would increase over time, leading to a more accurate, objective, and real-time tool for cervical cancer screening. With the availability of a larger data set, a supervised ML algorithm with SVM could be configured to classify different grades of cervical cancer, such as LSIL, HSIL, and CIN grades 1, 2, and 3, as well as carcinoma *in situ*. The SVM classifies the data by identifying the best line to separate data points, with the support vectors being the closest points to the hyperplane. These support vectors influence the position of hyperplane, leading to a more generalized cloud-based classification model. A similar cloud-based integration of an ML algorithm was utilized in the case of OralScan, an intraoral multimodal camera for oral cancer screening and biopsy guidance.[8] In this ML algorithm, the R610/R545 image intensity ratio was utilized to classify both normal and potentially malignant tissues, as well as normal versus abnormal tissues. This algorithm processed oral tissues from different anatomical sites in the oral cavity with diverse morphologies. The similarity of this study with our study is the use of R610/R545 image ratio value for cancer screening and biopsy guidance. The hypothesis is that the cervical and oral tissues are made of squamous epithelium, and hence, the optical features are expected to be similar.

In this study, the collagen fluorescence intensity was recorded in all patients using excitation at 370 nm. The recorded fluorescence images appeared dark, possibly due to the low penetration of ultraviolet light in cervical tissues. The stroma of the cervix, concealed by epithelial tissue, is the source of collagen fluorescence. Hence, the excitation light would find it difficult to reach the stroma residing below the basal layer of epithelium.[27] Furthermore, the absorption of the 370 nm light by other biochemical constituents of the cervix – which absorbs at this wavelength and emits with increased intensity during malignant transformations in the tissue – could also lead to an unpredictable fluorescence emission.[28]

In a recent study conducted on 160 patients, the sensitivity and specificity of the Pap smear test were observed to be 47.19% and 64.79%, respectively, for the detection of premalignant lesions of the cervix, and 64.72% and 52.74%, respectively, for colposcopy.[29] Although colposcopy shows a comparatively higher diagnostic accuracy, both of these modalities are subjective. In comparison, our DR imaging technique is objective, with the DR ratio value representing changes in the deoxy- and oxygenated Hb absorption. This ratio correlates with variations in backscattered light intensity due to changes at the cellular level.

The most common symptoms reported by patients enrolled in the study (Table A1) were abdominal pain and abnormal bleeding. Fewer patients had spotting, abnormal discharge, and irregular menstrual cycles. The presence of blood or moisture in the cervix could affect the DR image ratio values. These cervical conditions may cause light to reflect off the surface, resulting in specular reflection. The resulting ratio values from specular reflection can distort DR measurements. Therefore, when a patient has bleeding or experiences bleeding on touch, the DR ratio values may be misleading. This limitation can be minimized by cleaning the cervix before imaging. Another limitation of this study is the low number of malignant cases. Further multicenter studies are planned to improve the algorithm and develop a grade-specific classification.

During conventional cervical check-ups, most women who undergo a Pap smear test do not return to collect the reports, which are usually available in 2 weeks for further follow-up. The non-availability of real-time screening results is a significant drawback for screening modalities such as Pap smears or colposcopy-directed biopsies. The ability of the multimodal imaging system (CerviScan) to provide real-time results, with the help of an ML algorithm, presents a strong rationale for adopting this novel technology in screening women above 30 years of age. CerviScan can help to identify, locate, and treat CIN, while minimizing its possibility to progress to higher grades of CIN and reducing mortality. In addition, the capability of CerviScan to locate the most malignant site for biopsy enhances its value by providing a more accurate pathology. The real-time image ratio (R610/R545 and R610/R575) analytics and PCM display of autofluorescence, as well as HbO_2 absorption maps, help in the speedy assessment of malignant status and/or cervicitis.

5. Conclusion

Quantitative detection of cervical malignancies without the need for tissue incision holds great clinical significance. The algorithm developed for non-invasive multispectral widefield imaging using CerviScan provides an opportunity to objectively screen and detect cervical cancer in real time, while also assisting the gynecologist in locating the malignant site for biopsy. The cloud-based platform approach will present a more accessible and cost-effective solution for cervical cancer screening. The data from different centers, including patients with diverse age groups, menstrual phases, and gynecological histories, would refine the algorithm over time. As there are changes in the cervical anatomy during the menstrual span of women, age-specific algorithms would enhance the diagnostic accuracy. ML algorithms can outdo the interobserver variability among cytology results and could detect subtle cellular changes that might be missed by human experts. ML-powered digital diagnosis and ML-based screening would enable remote diagnosis in low-resource settings with limited access to specialists.

In this study, an overall diagnostic accuracy of 94% was achieved using the DR image ratio R610/R540 algorithm for the discrimination of malignant tissues from normal tissues. However, the data derived using collagen fluorescence could not lead to a confirmative diagnosis. Alternative markers relying on protoporphyrin IX fluorescence with excitation at 405 nm could be utilized, as in OralScan, to improve screening accuracy. Furthermore, the intensity and uniformity of illumination could be enhanced by the addition of more LEDs.

The mortality rates due to cervical cancer could be minimized by utilizing CerviScan in large-scale screening programs across the country. We believe that early detection of cervical cancer would reduce healthcare costs and minimize the number of patients lost during follow-up, as often occurs with traditional screening methods such as Pap smear and HPV deoxyribonucleic acid tests, which require a waiting period of 1 week to get the screening results. The potential of the device to screen and detect cervical cancers at the point-of-care in real time, along with its capability for biopsy guidance – without the need for visual inspection with acetic acid/visual inspection with Lugol's iodine staining – will improve patient compliance and its effectiveness as a novel modality for the early direction of cervical cancers.

Acknowledgments

The authors are grateful to acknowledge the support received from the Ethics Committee at the Kasturba Medical College (KMC), Manipal, India. The authors would like to thank Prof. Dr. Stanley Mathew, Department of Surgery, KMC, for his invaluable guidance and advice. The cooperation and support received from the enrolled patients was commendable.

Funding

The project was partially supported through a grant received under the ELEVATE 100 program of the Government of Karnataka in 2017.

Conflict of interest

The authors declare that they have no competing interests.

Author contributions

Conceptualization: Subhash Narayanan
Formal analysis: Phebe George, Rinoy Suvarnadas
Investigation: Phebe George, Rekha Upadhya

Methodology: Subhash Narayanan
Project administration: Rinoy Suvarnadas
Resources: Rekha Upadhya, Niranjana Sampthalia
Supervision: Subhash Narayanan
Writing – original draft: Phebe George
Writing – review & editing: Subhash Narayanan

Ethics approval and consent to participate

This study was approved by the Institutional Ethics Committee of Kasturba Medical College, Manipal, Karnataka, India (Ethics approval number: 152/2020). Written informed consent was obtained from all participants included in the study.

Consent for publication

All patients signed informed consent forms before enrollment in the study.

Availability of data

Data presented in this paper will be available from the corresponding author on reasonable request.

References

1. Ferlay J, Soerjomataram I, Dikshit R, *et al*. Cancer incidence and mortality worldwide: Sources, methods and major patterns in GLOBOCAN 2012. *Int J Cancer*. 2015;136(5):E359-E386.

   doi: 10.1002/ijc.29210

2. Denny L. Cervical cancer: Prevention and treatment. *Discov Med*. 2012;14(75):125-131.

3. Sankaranarayanan R, Ramadas K, Gauvreau CL, *et al*. Socioeconomic factors and cancer prevention in India: Diverse interventions are needed. In: Wild CP, Weiderpass E, Stewart BW, editors. *World Cancer Report: Cancer research for cancer prevention. Lyon (FR): International Agency for Research on Cancer.* Vol 4.4; 2020. Available from: https://www.ncbi.nlm.nih.gov/books/NBK606515/

4. Leyden WA, Manos MM, Geiger AM, *et al*. Cervical cancer in women with comprehensive health care access: Attributable factors in the screening process. *J Natl Cancer Inst*. 2005;97(9):675-683.

   doi: 10.1093/jnci/dji115

5. Barut MU, Kale A, Kuyumcuoğlu U, *et al*. Analysis of sensitivity, specificity, and positive and negative predictive values of smear and colposcopy in diagnosis of premalignant and malignant cervical lesions. *Med Sci Monit*. 2015;21:3860-3867.

   doi: 10.12659/MSM.895227

6. Rahmadwati G, Naghdy G, Ross M, Todd C, Norachmawati E. Classification of Cervical Cancer Using Histology Images. In: *2010 Second International Conference on Computer Engineering and Applications*. Bali, Indonesia: IEEE; 2010. p. 515-519.

   doi: 10.1109/ICCEA.2010.105

7. Bosch FX, Burchell AN, Schiffman M, *et al.* Epidemiology and natural history of human papillomavirus infections and type-specific implications in cervical neoplasia. *Vaccine*. 2008;26(Suppl 10):K1-K16.

   doi: 10.1016/j.vaccine.2008.05.064

8. Narayanan S, Anand S, Prasanna R, *et al.* Bimodal multispectral imaging system with cloud-based machine learning algorithm for real-time screening and detection of oral potentially malignant lesions and biopsy guidance. *J Biomed Opt*. 2021;26(8):086003.

   doi: 10.1117/1.JBO.26.8.086003

9. Prasad PN. *Introduction to Biophotonics*. 1st ed. United States: John Wiley and Sons; 2003.

10. Prabitha VG, Suchetha S, Jayanthi JL, *et al.* Detection of cervical lesions by multivariate analysis of diffuse reflectance spectra: A clinical study. *Lasers Med Sci*. 2016;31(1):67-75.

    doi: 10.1007/s10103-015-1829-z

11. Mirabal YN, Chang SK, Atkinson EN, Malpica A, Follen M, Richards-Kortum R. Reflectance spectroscopy for *in vivo* detection of cervical precancer. *J Biomed Opt*. 2002;7(4):587-594.

    doi: 10.1117/1.1502675

12. Shaikh R, Prabitha VG, Dora TK, *et al.* A comparative evaluation of diffuse reflectance and Raman spectroscopy in the detection of cervical cancer. *J Biophotonics*. 2016;10(2):242-252.

    doi: 10.1002/jbio.201500248

13. Prabitha VG, Suchetha S, Jayanthi JL, *et al.* Multi-spectral diffuse reflectance imaging for detection of cervical lesions: A pilot study. *Int J Eng Sci Innov Technol*. 2014;3(6):169-177.

14. Messadi DV, Younai FS, Liu HH, Guo G, Wang CY. The clinical effectiveness of reflectance optical spectroscopy for the *in vivo* diagnosis of oral lesions. *Int J Oral Sci*. 2014;6:162-167.

    doi: 10.1038/ijos.2014.39

15. Stephen MM, Jayanthi JL, Unni NG, *et al.* Diagnostic accuracy of diffuse reflectance imaging for early detection of pre-malignant and malignant changes in the oral cavity: A feasibility study. *BMC Cancer*. 2013;13:278.

    doi: 10.1186/1471-2407-13-278

16. Prasanth CS, Stephen MM, Dora TK, Maheshwari A, Subhash N. Non-invasive detection of periodontal disease using diffuse reflectance spectroscopy: A clinical study. In: *Biomedical Applications of Light Scattering VI*. Vol. 8230. Bellingham: SPIE; 2012. p. 117-127.

17. Prasanth CS, Betsy J, Jayanthi JL, Nisha UG, Prasantila J, Subhash N. *In vivo* inflammation mapping of periodontal disease based on diffuse reflectance spectral imaging: A clinical study. *J Biomed Opt*. 2013;18(2):026019.

doi: 10.1117/1.JBO.18.2.026019

18. Chandra Sekhar P, Betsy J, Presanthila J, Subhash N. Discrimination of periodontal diseases using diffuse reflectance spectral intensity ratios. *J Biomed Opt*. 2012;17(2):027001.

doi: 10.1117/1.JBO.17.2.027001

19. Barik AK, Pavithran MS, Nelliat M, *et al*. Laser induced fluorescence of cervical tissues: An *in vitro* study for the diagnosis of cervical cancer from the cervicitis. *J Opt*. 2022;24(5):054002.

doi: 10.1088/2040-8986/ac59e2

20. Zhang H, Chen C, Ma C, *et al*. Feature fusion combined with Raman spectroscopy for early diagnosis of cervical cancer. *IEEE Photonics J*. 2021;13(3):3900311.

doi: 10.1109/JPHOT.2021.3075958

21. Huang W, Sun S, Yu Z, Lu S, Feng H. Chronic cervicitis and cervical cancer detection based on deep learning of colposcopy images toward translational pharmacology. *Front Pharmacol*. 2022;13:911962.

doi: 10.3389/fphar.2022.911962

22. Dong B, Lu Z, Yang T, *et al*. Development, validation, and clinical application of a machine learning model for risk stratification and management of cervical cancer screening based on full-genotyping hrHPV test (SMART-HPV): A modelling study. *Lancet Reg Health West Pac*. 2025;55:101480.

doi: 10.1016/j.lanwpc.2025.101480

23. Wekalao J, Kumaresan MS, Mallan S, *et al*. Metasurface based surface plasmon resonance (SPR) biosensor for cervical cancer detection with behaviour prediction using machine learning optimization based on support vector regression. *Plasmonics*. 2024:1-24.

doi: 10.1007/s11468-024-02623-8

24. Sarhangi HA, Beigifard D, Farmani E, Bolhasani H. Deep learning techniques for cervical cancer diagnosis based on pathology and colposcopy images. *Inform Med Unlocked*. 2024;47:101503.

doi: 10.1016/j.imu.2024.101503

25. El-Nashar SA, Mariani A. Uterine carcinosarcoma. *Clin Obstet Gynecol*. 2011;54(2):292-304.

doi: 10.1097/GRF.0b013e31821ac635

26. Gupta N, Dudding N, Smith JHF. Eight cases of malignant mixed Müllerian tumor (carcinosarcoma) of the uterus: Findings in SurePath™ cervical cytology. *Diagn Cytopathol*. 2014;42(2):165-169.

doi: 10.1002/dc.22910

27. Arbyn M, Weiderpass E, Bruni L, *et al*. Estimates of incidence and mortality of cervical cancer in 2018: A worldwide analysis. *Lancet Glob Health*. 2020;8(2):e191-e203.

doi: 10.1016/S2214-109X(19)30482-6

28. Nordstrom RJ, Burke L, Niloff JM, Myrtle JF. Identification of cervical intraepithelial neoplasia (CIN) using UV-excited fluorescence and diffuse-reflectance tissue spectroscopy. *Lasers Surg Med*. 2001;29(2):118-127.

doi: 10.1002/lsm.1097

29. Najib FS, Hashemi M, Shiravani Z, Poordast T, Sharifi S, Askary E. Diagnostic accuracy of cervical pap smear and colposcopy in detecting premalignant and malignant lesions of cervix. *Indian J Surg Oncol*. 2020;11(3):453-458.

doi: 10.1007/s13193-020-01118-2

Appendix

Table A1. Patient details, obstetric history, clinical symptoms, physical findings, histopathology results, and the image intensity ratio values (R610/R545 and R610/R575)

Patient no.	Age	Obstetric history	Menopausal status	Symptoms	Physical findings of examination	Histopathology results	R610/ R545	R610/ R575
1	50	P3L3	Pre	Difficulty in passing urine	Unhealthy cervix; cervical erosion observed	Chronic cervicitis with no dysplasia	1.461	2.433
2	64	P3L3	Post	History of foul-smelling discharge	UV prolapse	Normal	1.329	1.412
3	46	P2L2	Pre	Abdominal pain	Healthy cervix	Normal	1.307	1.408
4	53	P3L3	Pre	Abdominal pain; heavy menstrual bleeding	Endocervical polyp; bleeds on touch	Chronic cervicitis		1.73
5	45	P3L3	Pre	Abdominal distension	Healthy cervix	Normal	1.219	1.41
6	41	P2L2	Pre	Irregular spotting; breast pain during menstrual cycles	Polyp from the cervical canal; bleeds on touch	Chronic cervicitis with no dysplasia	1.263	1.708
7	43	P2L2	Pre	Abdominal pain; amenorrhea	Healthy cervix	Normal	1.112	1.583
8	49	Nulliparous	Pre	Abdominal pain; heavy menstrual bleeding	Erosions present; bleeding from the cervical os	Normal	1.401	1.463
9	47	P1L1	Pre	Heavy menstrual bleeding	Healthy cervix; copious amount of bleeding present	Chronic cervicitis with no dysplasia	1.28	1.845
10	49	P2L2	Pre	Lower abdominal pain; menstrual cramps	Indurated cervix; endometrial polyp present	Chronic cervicitis		2.227
11	47	P2L2	Pre	Burning micturition; continuous spotting; mass in descending pelvis	Healthy cervix; hypertrophied anterior lip with grade 1 descent	Chronic papillary endocervicitis		1.954
12	43	P2L2	Pre	Heavy menstrual bleeding; irregular cycles; mass per vagina	Healthy and elongated cervix; second-degree UV prolapse	Chronic papillary cervicitis		1.677
13	34	P2L2	Pre	On and off abdominal pain	Unhealthy, hypertrophied cervix with erosions; small cervical polyp; mass per vagina; third-degree UV prolapse	Normal	1.26	1.02
14	48	P2L2	Post	Abdominal pain;	WDPV; cervical erosions present;	Normal	1.328	1.507
15	29	P4 L3	Pre	itching in the perineal region; mass per vagina; second-degree of UV prolapses	elongated and hypertrophied cervix	Normal	1.226	1.348
16	53	P2L2	Pre	Itching in the vulval region; lower abdominal pain; dysuria	Cervix pulled up	Inflammatory infiltrate with no dysplasia	1.12	1.732
17	58	P3L3	Pre	Heavy menstrual bleeding		Low-grade squamous intraepithelial CIN-I	1.688	
18	45	P2L2	Pre	Heavy menstrual bleeding; frequent cycles	Healthy cervix; adenofibroma on posterior wall	Normal	1.212	1.188
19	37	P2L2	Pre	Heavy menstrual bleeding; irregular cycles	Bulky cervix	Chronic cervicitis with squamous metaplasia	1.414	1.812
20	47	P2L2	Pre	Heavy menstrual bleeding	Healthy cervix	Normal	1.49	1.32

(Cont'd...)

Table A1. ***(Continued)***

Patient no.	Age	Obstetric history	Menopausal status	Symptoms	Physical findings of examination	Histopathology results	R610/R545	R610/R575
21	41	P2L2	Pre	Heavy menstrual bleeding	Bulky cervix; shaped slit; mucoid discharge	Chronic cervicitis with squamous metaplasia	1.381	1.584
22	52	P2L2	Pre	Lower abdominal pain; spotting; back pain; bleeding from the cervical os	Healthy cervix	Chronic inflammation and cervix-free carcinoma	2.11	1.885
23	56	P2L2	Post	Post-menopausal bleeding; abdominal pain	Mass lesion in the lower vaginal cavity; stenosis of the vaginal cavity	Moderately differentiated SCC Grade 2	2.078	
24	50	P1L1	Pre	Foul-smelling blood stain; abdominal pain; general weakness; WDPV; loss of appetite	6 – 7 cm growth on the anterior side of the cervix; growth observed from the cervix into the vagina	Carcinosarcoma	3.005	
25	42	P4L2CO2	Pre	Lower abdominal pain; foul-smelling watery discharge	Hard growth on the lower lip of the cervix; cervical os is not visible; bleeds on touch	Moderately differentiated invasive SCC Grade 2	1.769	
26	76	P5L5	Post	Post-menopausal bleeding	Cervical wounds	Normal	1.499	1.417
27	50	P3L3	Post	Lower abdominal pain	Ovarian cyst	Chronic cervicitis		1.464
28	46	P1L1	Pre	Asymptomatic, abdominal tightness	Healthy cervix	Normal	1.196	1.211
29	75	P4L2CD2Ab4	Post	WDPV; foul-smelling discharge	Healthy cervix	Normal	1.41	1.441
30	49	P3L3	Pre	Heavy menstrual bleeding	Healthy cervix with grade 1 descent	Normal	1.448	1.209
31	42	P2L2	Pre	Abdominal pain	Mass in descending pelvis	Chronic cervicitis with no dysplasia	1.396	1.186
32	48	P2L2	Pre	Burning micturition; itching around the labia	WDPV; cervical anterior lip erosions present	Normal	1.464	1.143
33	49	P7L7Ab1	Post	Abdominal pain	Minimal erosion	Chronic cervicitis with no malignancy		1.277
34	71	P8L6CD2	Post	Abdominal pain	Healthy cervix	Normal	1.344	1.259
35	45	P2L2	Pre	Heavy menstrual bleeding	Healthy cervix; bleeding from the cervical os	Leiomyoma and chronic cervicitis		1.166
36	39	P1L1Ab2	Pre	Tiredness; minimal WDPV	Healthy cervix	High-grade squamous intraepithelial lesion CIN grade 2 – 3	1.495	
37	53	P2L2	Post	Mass per vagina	Healthy cervix; second-degree prolapses	Chronic cervicitis with no dysplasia	1.327	1.283
38	32	P2L2 LSCS	Pre	Heavy menstrual bleeding		Chronic cervicitis		1.31
39	51	P2L2	Post	Lower abdominal pain; post-menopausal bleeding	Healthy cervix	Normal	1.412	0.965
40	58	P3L3	Post	Post-menopausal bleeding	Unhealthy cervix; bleeds on touch	Keratinizing moderately differentiated SCC	1.481	
41	74	P5L4D1	Post	Abdominal pain; back pain; WDPV	2 cm hard mass lesion; bleeds on touch; clinical stage 3B	Moderately differentiated SCC	1.585	
42	55	P3L3	Post	Post-menopausal bleeding; back pain	Present of erosions on the posterior cervix	Normal	1.39	0.499

Abbreviations: SCC: Squamous cell carcinoma; UV: Uterovaginal; WDPV: White discharge per vagina.